Inorganic Chemistry

Article

pubs.acs.org/IC

Iodide Ion Pairing with Highly Charged Ruthenium Polypyridyl Cations in CH_3CN

Wesley B. Swords, Guocan Li, and Gerald J. Meyer*

Department of Chemistry, University of North Carolina at Chapel Hill, Chapel Hill, North Carolina 27599-3290, United States

Supporting Information

ABSTRACT: A series of three highly charged cationic ruthenium(II) polypyridyl complexes of the general formula $[Ru(deeb)_{3-x}(tmam)_x](PF_6)_{2x+2}$, where deeb is 4,4′-diethyl ester-2,2′-bipyridine and tmam is 4,4′-bis[(trimethylamino)-methyl]-2,2′-bipyridine, were synthesized and characterized and are referred to as **1**, **2**, or **3** based on the number of tmam ligands. Crystals suitable for X-ray crystallography were obtained for the homoleptic complex **3**, which was found to possess D_3 symmetry over the entire ruthenium complex. The complexes displayed visible absorption spectra typical of metal-to-ligand charge-transfer (MLCT) transitions. In acetonitrile, quasi-reversible waves were assigned to $Ru^{III/II}$ electron transfer, with formal reduction potentials that shifted negative as the number of tmam ligands was increased. Room temperature photoluminescence was observed in acetonitrile with quantum yields of $\phi \sim 0.1$ and lifetimes of $\tau \sim 2$ μs. The spectroscopic and electrochemical data were most consistent with excited-state localization on the deeb ligand for **1** and **2** and on the tmam ligand for **3**. The addition of tetrabutylammonium iodide to the complexes dissolved in a CH_3CN solution led to changes in the UV−vis absorption spectra consistent with ion pairing. A Benesi−Hildebrand-type analysis of these data revealed equilibrium constants that increased with the cationic charge **1** < **2** < **3** with K = 4000, 4400, and 7000 M^{-1}. ^1H NMR studies in CD_3CN also revealed evidence for iodide ion pairs and indicated that they occur predominantly with iodide localization near the tmam ligand(s). The diastereotopic H atoms on the methylene carbon that link the amine to the bipyridine ring were uniquely sensitive to the presence of iodide; analysis revealed that an iodide "binding pocket" exists wherein iodide forms an adduct with the 3 and 3′ bipyridyl H atoms and the quaternized amine. The MLCT excited states were efficiently quenched by iodide. Time-resolved photoluminescence measurements of **1** revealed a static component consistent with rapid electron transfer from iodide in the "binding pocket" to the Ru metal center in the excited state, $k_{et} > 10^8$ s^{-1}. The possible relevance of this work to solar energy conversion and dye-sensitized solar cells is discussed.

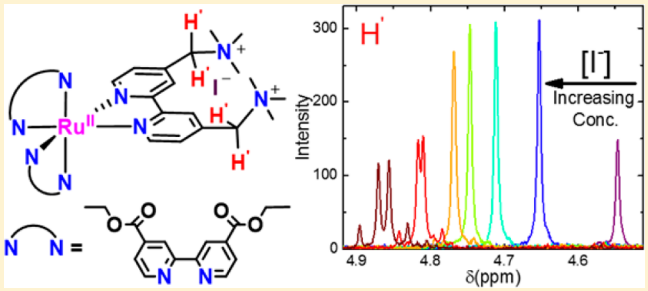

INTRODUCTION

The yields and dynamics of photoinduced electron-transfer reactions between donors and acceptors in a fluid solution are known to be influenced by Coulombic forces.[1] It has become increasingly apparent that ionic charges also play critical roles in the efficiency of dye-sensitized solar cells based on mesoporous thin films of anatase TiO_2 nanocrystallites.[2,3] Cations present in the electrolyte are known to be important for excited-state injection, regeneration of the oxidized dye, and transport of the injected electron to the external circuit.[2] Because these ions influence so many different aspects of the solar cell, it is often difficult to isolate and study a specific phenomenon. For example, surface adsorption of potential determining Lewis acidic cations such as Li^+ is known to influence the energy levels of the acceptor states in TiO_2, and the same cations have also recently been shown to screen the electric fields generated by excited-state injection.[4−6] Much less is known about how solar conversion efficiencies are influenced by the overall charge of the dye molecules, termed sensitizers. This is remarkable when one considers the vast research efforts in this area and the fact that the accepted mechanism for sensitizer regeneration after excited-state injection involves a putative ion pair between the oxidized dye and iodide.[7] This paper describes the synthesis and characterization of ruthenium(II) polypyridyl complexes with 4+, 6+, and 8+ charges that display enhanced ion pairing and excited-state reactivity with iodide.

In one of the very few studies to address the importance of sensitizer charge, Nazeeruddin and co-workers reported careful titration experiments that enabled the characterization and isolation of three different protonation states of N3, *cis*-$Ru(dcb)_2(NCS)_2$, where dcb is 2,2′-bipyridine-4,4′-dicarboxylic acid.[8] It was found that the sensitizer with two of the four carboxylic acid groups deprotonated, termed N719, gave rise to the highest solar energy conversion efficiency. If the 2− charge of N719 was maintained upon surface binding, then the oxidized form would be a 1− anion unlikely to ion pair with iodide. As was pointed out by these authors, the presence of acidic protons shifts the TiO_2 conduction band away from the vacuum level, which can lower the open-circuit photovoltage

Received: February 11, 2015
Published: April 14, 2015

DOI: 10.1021/acs.inorgchem.5b00344
Inorg. Chem. 2015, 54, 4512−4519

and solar energy conversion efficiency. Therefore, while N3 could transfer four protons to TiO_2, N719 transferred only two. Hence, Brønsted acid−base surface chemistry complicated analysis of the role of charge in this study, and it is likely that N3 and all of the conjugate bases derived from it were fully deprotonated when anchored to the TiO_2 surface.[8]

Indeed, to our knowledge, all of the attenuated total reflectance Fourier transfer infrared studies of transition-metal sensitizers with dcb ligand(s) reveal complete deprotonation when anchored to a TiO_2 surface from organic solvents.[2] An asymmetric CO stretch is observed near 1610 cm^{-1}, which is most consistent with carboxylate binding.[9−11] Therefore, surface-anchored *cis*-$Ru(dcb)_2(NCS)_2$ possesses a 4− total charge in the ground and excited states and a 3− charge after excited-state injection regardless of which protonation state is initially anchored to the surface. Unfortunately, in this literature, the oxidized sensitizers are often referred to as "dye cations" even though the best available data indicate that champion Ru^{II} sensitizers remain anionic after excited-state injection.[12,13] It is not clear whether an oxidized sensitizer anchored to TiO_2 has ever held a cationic charge. As a result, it is of interest to characterize sensitizers with high cationic charges to more fully understand the importance of the sensitizer charge and the possible interfacial ion pairing with iodide. This paper describes the first studies directed toward this goal.

Herein a series of three complexes of the general formula $[Ru(deeb)_{3-x}(tmam)_x](PF_6)_{2x+2}$ were synthesized and characterized and are referred to by the number of 4,4′-bis[(trimethylamino)methyl]-2,2′-bipyridine (tmam) ligands, x = 1 (**1**), 2 (**2**), or 3 (**3**). The ligands are shown in Scheme 1. The 4,4′-diethyl ester-2,2′-bipyridine (deeb) ligand was chosen because the ethyl ester groups can later be saponified for studies at TiO_2 interfaces. The tmam ligand has a 2+ charge by virtue of the quaternary alkylated amine substituents in the 4 and 4′ positions of the bipyridine ligand. This cationic ligand is shown to influence the redox properties of the complexes as well as the metal-to-ligand charge-transfer (MLCT) excited states. The tmam ligand also enhances ion pairing with iodide, as evidenced by ^{1}H NMR, UV−vis, and photoluminescence (PL) titration studies. Significantly, the tmam ligand appears to provide a specific "binding pocket" for iodide that facilitates rapid photooxidation. To our knowledge, complex **3** is the most highly charged mononuclear ruthenium(II) complex reported.

Scheme 1. tmam and deeb Ligands Utilized in This Paper

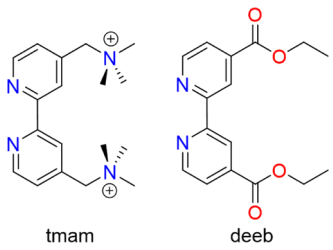

EXPERIMENTAL SECTION

Materials. Argon gas (Airgas, 99.998%) was passed through a Drierite drying tube before use. Acetonitrile (Burdick and Jackson, 99.98%), acetone (Aldrich, 99.5%), dichloromethane (DCM; Fisher, 99.5%), diethyl ether (Aldrich, 99.5%), ethanol (Fisher, 200 proof, 99.5%), and methanol (Aldrich, 99.5%) were used as received. Ammonium hexafluorophosphate, dichloro(*p*-cymene)ruthenium(II) dimer (Ru-dimer), 48% hydrobromic acid, lithium perchlorate, silver hexafluorophosphate, silver nitrate, sodium borohydride, sulfuric acid, tetrabutylammonium iodide (TBAI), tetrabutylammonium perchlorate, and 45% aqueous trimethylamine were purchased from Aldrich and used as received. 4,4′-Diethyl ester-2,2′-bipyridine (deeb) was prepared according to the literature procedure.[14]

NMR. Characteristic NMR spectra were obtained using Bruker Avance III 400 MHz (^{1}H) and 600 MHz (^{13}C) spectrometers. NMR spectra were referenced to the central line of the solvent (CD_3CN) and processed using MNOVA.

Mass Spectrometry. Electrospray ionization mass spectrometry (ESI-MS) data were collected on a Micromass Triple Quadrupole mass spectrometer with a Z-spray nanoelectrospray source and sampled by an Advion TriVersa NanoMate sampling system. Measurements were made on complexes dissolved in acetonitrile. The complexes were identified by their multiple ionization peaks.

X-ray Diffraction. A suitable crystal was selected and mounted on a MITIGEN holder in paratone oil on a Bruker APEX-II CCD diffractometer. The crystal was kept at 100 K during data collection. Using *Olex2*, the structure was solved with the *olex2.solve* structure solution program using charge flipping and refined with the XL refinement package using least-squares minimization.[15−17]

UV−Vis Absorption. UV−vis absorption spectra were recorded using Varian Cary 50 and 60 UV−vis spectrophotometers with a resolution of 1 nm.

Steady-State PL. Steady-state PL spectra were recorded using an ISS K2 fluorimeter. Samples were sparged with argon for 20 min and excited at the MLCT absorption maximum (typically $\lambda \sim 460$ nm). The intensity was integrated for 0.5 s at 4 nm resolution. PL quantum yields were measured through comparative actinometry using $[Ru(bpy)_3][PF_6]_2$ in acetonitrile (ϕ_{em} = 0.062) as a quantum yield standard.[18]

Time-Resolved PL. Lifetimes and time-resolved PL single-wavelength decays were acquired on a nitrogen dye laser with excitation centered at 500 nm. Decays were monitored at the PL maximum and averaged over 180 scans.

Electrochemistry. Cyclic voltammetry (CV) experiments were performed with a BASi CV-50W voltammetric analyzer using a standard three-cell setup. Cells used consisted of platinum, gold, glassy carbon, or mercury working electrodes with platinum mesh, disk, or wire auxiliary electrodes and aqueous silver/silver chloride reference electrodes from Pine Instrumentation and BASi Analytical Instrumentation (mercury electrode only). A BASi controlled-growth mercury electrode on the standing drop setting was used as the working mercury electrode. Supporting electrolytes of 300 mM $LiClO_4$ or $TBAClO_4$ in acetonitrile were used for all measurements. The reference electrodes were referenced to an external ferrocene standard (630 mV vs NHE) before and after each series of measurements.[19]

Iodide Titrations. Titrations were performed on complexes **1**−**3** in CH_3CN with a fixed ruthenium concentration and variable concentrations of TBAI. ^{1}H NMR titrations were performed on a Bruker Avance III 500 MHz spectrometer. Titrations were performed with ∼2 mM ruthenium and $^1/_2$ equiv additions of TBAI. Each spectrum was averaged over 32 scans. UV−vis titrations were performed with ∼50 μM ruthenium titrated with $^1/_4$ equiv of TBAI. PL titrations were completed using the same sample for both steady-state and time-resolved measurements. The solutions were excited at 500 nm, where absorbance changes were minimal. Solutions of ∼25 μM ruthenium were titrated with $^1/_4$ equiv of TBAI. Data analysis for all experiments was performed using *OriginLab*, version 9.0.

4,4′-Bis[(trimethylamino)methyl]-2,2′-bipyridine Bis(hexafluorophosphate) (tmam). The following synthesis of tmam was modified from Li et al., shown in Scheme 2.[20] Reduction of deeb with sodium borohydride in refluxing ethanol gave 4,4′-dihydroxymethyl-2,2′-bipyridine in 81% yield. Continued refluxing in 48% hydrobromic acid with catalytic sulfuric acid produced 4,4′-dibromomethyl-2,2′-bipyridine in 72% yield. To a stirring solution of 4,4′-dibromomethyl-2,2′-bipyridine (207 mg, 0.660 mol) in 10 mL of ethanol was added 1.5 mL (excess) of 45% aqueous trimethylamine

DOI: 10.1021/acs.inorgchem.5b00344
Inorg. Chem. 2015, 54, 4512−4519

Scheme 2. Synthetic Procedure for the tmam Ligand

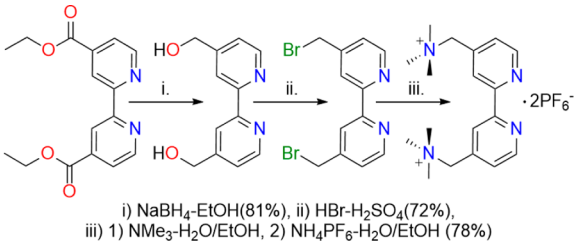

dropwise. The cloudy solution was stirred at room temperature where it transitioned to clear and back to cloudy over 1 h. Deionized (DI) water was added dropwise until the solution became clear. A large excess of ammonium hexafluorophosphate was added, precipitating tmam. Collection over a fine frit, washing with DI water, and drying under vacuum gave a light-pink-gray powder, yielding 280 mg (78%). The overall yield from deeb to tmam was 45%. ^{1}H NMR (CD_3CN): δ 8.84 (d, 2H, J = 4.0 Hz), 8.58 (d, 2H, J = 1.0 Hz), 7.56 (dd, 2H, J = 4.0 and 1.6 Hz), 4.50 (s, 4H), 3.09 (s, 9H). ^{13}C NMR (CD_3CN): δ 53.9, 68.7, 125.3, 128.9, 138.3, 151.5, 157.1.

[Ru(*p*-cymene)(deeb)Cl]Cl. Modified from Yu et al., [Ru(*p*-cymene)(deeb)Cl]Cl was synthesized by the addition of Ru-dimer (201 mg, 0.329 mmol) and deeb (198 mg, 0.657 mmol) to a 25 mL round-bottomed flask.[21] After the addition of 1:1 DCM/acetone (8 mL), the slurry was sparged with nitrogen for 20 min and refluxed under dinitrogen for 3 h with little color change. Removal of solvent yielded an orange product, which was slurried in DI water and filtered. Removal of DI water under vacuum gave 323 mg of the desired product (81% yield). ^{1}H NMR (CD_3CN): δ 9.87 (dd, 2H, J = 6.0 and 0.8 Hz), 8.84 (d, 2H, J = 1.6 Hz), 8.13 (dd, 2H, J = 8.0 and 1.6 Hz), 6.22 (d, 2H, J = 6.4 Hz), 6.03 (d, 2H, J = 6.4 Hz), 4.46 (q, 4H, J = 7.2 Hz), 2.67 (hept, 1H, J = 6.8 Hz), 1.42 (t, 6H, J = 6.8 Hz), 1.01 (d, 6H, J = 7.2 Hz). ^{13}C NMR (CD_3CN): δ 14.4, 19.0, 22.2, 31.8, 63.7, 83.2, 88.3, 105.6, 107.01, 124.1, 127.6, 141.8, 155.9, 158.3, 164.0.

[Ru(*p*-cymene)(tmam)Cl][PF$_6$]$_2$Cl. A total of 2 equiv of tmam (150 mg, 0.254 mol) and Ru-dimer (78 mg, 0.127 mmol) were dissolved in acetone (8 mL) in a 25 mL round-bottomed flask and sparged with nitrogen for 20 min. The solution was refluxed for 3 h under dinitrogen, changing from red to yellow. After cooling to room temperature, a yellow precipitate formed. Filtering over a fine frit and drying under vacuum yielded 181 mg (80%) of the desired product. ^{1}H NMR (CD_3CN): δ 9.49 (d, 2H, J = 5.6 Hz), 9.19 (s, 2H), 7.89 (dd, 2H, J = 5.6 and 1.6 Hz), 5.99 (d, 2H, J = 6.4 Hz), 5.84 (d, 2H, J = 6.4 Hz), 4.80 (m, 4H), 3.23 (s, 18H), 2.72 (hept, 1H, J = 6.8 Hz), 2.16 (s, 3H), 1.08 (d, 6H, J = 6.8 Hz). ^{13}C NMR (CD_3CN): δ 18.8, 22.2, 31.9, 54.5, 67.9, 86.3, 87.2, 129.9, 130.1, 132.0, 140.4, 141.2, 156.38, 156.96.

[Ru(tmam)(deeb)$_2$][PF$_6$]$_4$ (1). To a 25 mL round-bottomed flask was added [Ru(*p*-cymene)(tmam)Cl][PF$_6$]$_2$Cl (19.5 mg, 0.0223 mmol), 2 equiv of deeb (13.4 mg, 0.0446 mol), and a slight excess of silver hexafluorophosphate (13.4 mg, 0.0480 mmol). Ethanol (6 mL) and acetone (2 mL) were added and sparged with nitrogen for 20 min. The mixture was refluxed under dinitrogen over 2 days, while the color changed from yellow to red. The reaction was filtered over a fine frit. Removal of solvent under vacuum yielded an orange solid, which was dissolved in DI water and filtered. The DI water was removed under vacuum, yielding 15 mg (43%) of **1** as a red powder. ^{1}H NMR: δ 9.07 (m, 4H), 8.56 (d, 2H, J = 1.2 Hz), 7.93 (d, 2H, J = 6.0 Hz), 7.88 (dd, 2H, J = 6.0 and 1.6 Hz), 7.86 (d, 2H, J = 6.0 Hz), 7.83 (m, 4H), 7.51 (dd, 2H, J = 5.6 and 1.6 Hz), 4.52 (s, 4H), 4.47 (dq, 8H, J = 4.0 and 7.2 Hz), 3.13 (s, 18H), 1.41 (dt, 12H, J = 4.0 and 7.2 Hz). ^{13}C NMR (CD_3CN): δ 14.4, 54.2, 63.8, 63.8, 67.7, 124.8, 124.9, 127.7, 127.9, 129.2, 132.3, 139.2, 140.6, 140.7, 153.9, 154.0, 154.3, 158.1, 158.2, 158.3, 164.3, 164.4. ESI-MS. Calcd (found) for $RuC_{50}H_{60}N_8O_8P_3F_{18}$: m/z^+ 1437.02 (1437.35). Calcd (found) for $RuC_{50}H_{60}N_8O_8P_2F_{12}$: m/z^{2+} 646.03 (646.23). Elem anal. Calcd for $RuC_{50}H_{60}N_8O_8P_4F_{24}$ (1581.98): C, 37.96; H, 3.82; N, 7.08. Found: C, 37.12; H, 3.84; N, 7.00.

[Ru(tmam)$_2$(deeb)][PF$_6$]$_6$ (2). To a 25 mL round-bottomed flask were added [Ru(*p*-cymene)(deeb)Cl]Cl (10.1 mg, 0.0169 mmol), 2 equiv of tmam (19.6 mg, 0.0339 mmol), and a slight excess of silver nitrate (7.0 mg, 0.0412 mmol) along with 6 mL of ethanol. The mixture was sparged with nitrogen for 20 min and refluxed over 2 days, during which the color changed from orange to brown. The reaction mixture was filtered over a fine frit, yielding a brown-orange precipitate, which was dissolved in acetonitrile and filtered over a fine frit. Removal of the solvent under vacuum gave a red-orange powder. This powder was redissolved in acetonitrile, and a large excess of ammonium hexafluorophosphate was added. Acetonitrile was removed under vacuum, and the remaining solid was slurried in ethanol, filtered, and dried under vacuum. Recrystallization by vapor diffusion of methanol into a concentrated acetonitrile solution yielded 15 mg (47%) of **2**. ^{1}H NMR: δ 9.07 (d, 2H, J = 0.8 Hz), 8.62 (dd, 4H, J = 5.6 and 1.2 Hz), 7.91 (d, 4H, J = 4.4 Hz), 7.88 (dd, 2H, J = 4.8 Hz), 7.81 (d, 2H, J = 4.8 Hz), 7.55 (dd, 2H, J = 4.8 and 1.6 Hz), 7.50 (dd, 2H, J = 4.8 and 1.6 Hz), 4.55 (s, 4H), 4.53 (s, 4H), 4.47 (q, 4H, J = 5.6 Hz), 3.14 (s, 18H), 3.12 (s, 18H), 1.41 (t, 6H, J = 5.6 Hz). ^{13}C NMR: δ 30.9, 38.0, 54.1, 54.2, 67.65, 67.67, 124.8, 127.9, 129.2, 129.3, 132.2, 132.4, 139.1, 139.1, 140.2, 153.8, 154.1, 154.2, 158.0, 158.2, 158.3, 164.9. ESI-MS. Calcd (found) for $RuC_{52}H_{72}N_{10}O_4P_5F_{30}$: m/z^+ 1727.08 (1727.15). Calcd (found) for $RuC_{52}H_{72}N_{10}O_4P_4F_{24}$: m/z^{2+} 791.09 (791.03). Elem anal. Calcd for $RuC_{52}H_{72}N_{10}O_4P_6F_{36}$ (1872.05): C, 33.36; H, 3.88; N, 7.48. Found: C, 31.88; H, 3.97; N, 7.30.

[Ru(tmam)$_3$][PF$_6$]$_8$ (3). To a 25 mL round-bottomed flask was added [Ru(*p*-cymene)(tmam)Cl][PF$_6$]$_2$Cl (20 mg, 0.224 mmol), 2 equiv of tmam (26.5 mg, 0.0448 mmol), and a small excess of silver hexafluorophosphate (17.2 mg, 0.0493 mmol) along with 6 mL of ethanol and 10 mL of acetone. The mixture was refluxed over 2 days, changing from yellow to red. The reaction mixture was filtered over a fine frit to isolate a brown powder. The powder was washed with acetonitrile to dissolve only the product. Removal of the solvent under vacuum yielded 17 mg of **3** (35%) as an orange powder.

An alternative synthesis was performed using an Anton Parr Monowave 300 microwave reactor. To a 10 mL microwave tube was added [Ru(*p*-cymene)(tmam)Cl][PF$_6$]$_2$Cl (68 mg, 0.0758 mmol), along with tmam (93.0 mg, 0.158 mmol) and 6 mL of DI water. The slurry was reacted at 150 °C for 2 h, during which the yellow slurry turned into a red solution. The reaction mixture was filtered through a fine frit, and an excess of ammonium hexafluorophosphate was added to precipitate orange solid **3**. The precipitate was isolated on a fine frit, washed with water and ethanol, and dried under vacuum, yielding 118 mg (72%). X-ray-quality crystals were grown out of acetonitrile through vapor diffusion of diethyl ether. ^{1}H NMR: δ 8.38 (d, 6H, J = 2 Hz), 7.88 (d, 6H, J = 6 Hz), 7.55 (dd, 6H, J = 6 and 2 Hz), 4.54 (s, 12H), 3.14 (s, 54H). ^{13}C NMR: δ 54.1, 67.6, 129.0, 132.3, 38.8, 154.0, 158.1. ESI-MS. Calcd (found) for $RuC_{54}H_{84}N_{12}P_6F_{36}$: m/z^{2+} 936.11 (936.19). Calcd (found) for $RuC_{54}H_{84}N_{12}P_5F_{30}$: m/z^{3+} 575.75 (575.87). Elem anal. Calcd for $RuC_{54}H_{84}N_{12}P_8F_{48}$ (2162.15): C, 30.00; H, 3.92; N, 7.78. Found: C, 30.04; H, 4.01; N, 7.63.

RESULTS

A modified literature procedure was used to obtain tmam in 45% yield.[5] Ligation of ruthenium proceeded through reaction with a known ruthenium dimer and gave the [Ru(LL)(*p*-cymene)Cl]Cl intermediate in high yield (LL = tmam or deeb). Further reaction with 2 equiv of tmam or deeb under reflux or high-temperature microwaving led to the isolation of **1**–**3** in 43%, 47%, and 72% yield, respectively. The identity of the complexes was confirmed using ^{1}H and ^{13}C NMR, mass spectrometry, and elemental analysis.

Crystals of **3** that were of sufficient quality for characterization by single-crystal X-ray crystallography were isolated (Figure 1). The expected stoichiometry of eight PF_6^- anions per Ru center was observed, although the PF_6^- anions were omitted from Figure 1 for clarity. The average Ru–N bond

DOI: 10.1021/acs.inorgchem.5b00344
Inorg. Chem. 2015, 54, 4512–4519

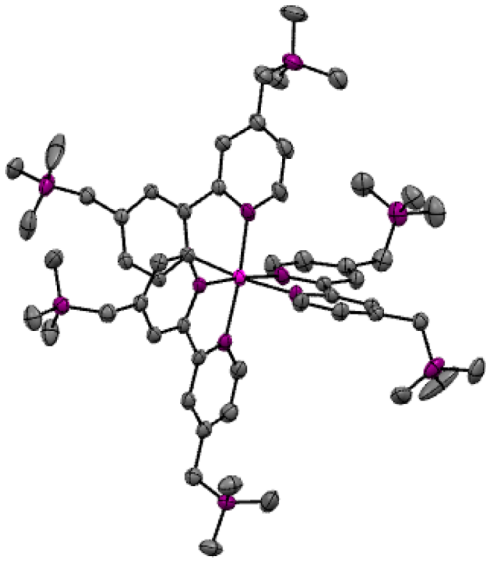

Figure 1. Displacement ellipsoid plot (50% probability level) for the cation **3**, $[Ru(tmam)_3]^{8+}$, obtained from single-crystal structure determination. The eight PF_6^- anions have been masked for clarity. Color code: pink, Ru; purple, N; gray, C.

distance was 2.063 Å. The average bite angle was 79.21°, and average N−Ru−N angles were 93.69 and 173.63°. The trimethylamine groups were oriented on opposite faces of the bipyridine rings, and the complex still maintained an overall D_3 point group, with the C_3 axis intersecting two faces of the octahedron and three C_2 axes through each bipyridine. Additional X-ray crystallographic data are included in Table 1.

Table 1. Crystal Parameters for 3

empirical formula	$C_{58}H_{90}F_{48}N_{14}P_8Ru$
fw	2244.26
temperature/K	100
cryst syst	monoclinic
space group	*C*2/*c*
a/Å	14.3741(7)
b/Å	30.0594(13)
c/Å	21.7725(9)
α/deg	90
β/deg	92.048(3)
γ/deg	90
volume/Å^3	9401.4(7)
Z	4
ρ_{calc}/(g/cm^3)	1.586
μ/mm^{-1}	3.920
cryst size/mm^3	0.354 × 0.12 × 0.057
radiation	Cu K*α* (*λ* = 1.54178)
final *R* indexes [$I > 2\sigma(I)$]	R1 = 0.0517, wR2 = 0.1342
final *R* indexes [all data]	R1 = 0.0691, wR2 = 0.1423

All characterization was performed in acetonitrile, under an argon atmosphere, and at room temperature, except where otherwise stated. The UV−vis spectra displayed absorption bands at 460 and 440 nm, which were assigned as MLCT transitions (Figure 2). An increase in the extinction coefficients was observed as the number of tmam ligands increased from 1 → 2 → 3. The intense band at 300 nm was assigned as a ligand-localized $\pi-\pi^*$ transition.

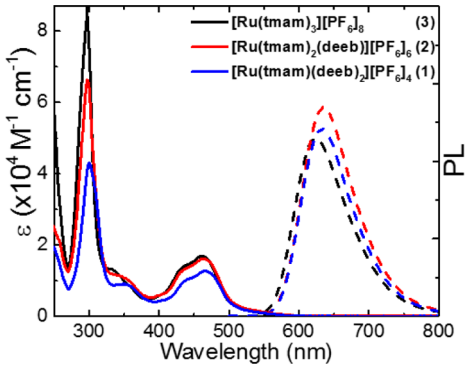

Figure 2. Steady-state absorption (solid line) and PL (dashed line) spectra for the indicated complexes in CH_3CN.

Light excitation into the MLCT absorption bands resulted in orange-red PL, which was visible to the dark adapted eye (Figure 2). Both **1** and **2** displayed maxima that were red-shifted ~260 cm^{-1} from that of **3**. Quantum yields were calculated through the optically dilute technique with $[Ru(bpy)_3][PF_6]_2$ in CH_3CN as a quantum yield standard.[18] Pulsed-laser excitation resulted in time-resolved PL data that were well described by a first-order kinetic model. Both the lifetime measurements and quantum yields were performed in triplicate and averaged to ensure accuracy, with uncertainty expressed in the last significant digit. Nonradiative and radiative rate constants were calculated using the corresponding quantum yields, $\phi = k_r/(k_r + k_{nr})$ and lifetimes, $\tau_0 = 1/(k_r + k_{nr})$. The photophysical properties of the complexes are given in Table 2.

Table 2. Photophysical Properties for 1−3 in CH_3CN

complex	MLCT abs max (nm)	PL max (nm)	τ_0 (μs)	ϕ	k_r (×10^4 s^{-1})	k_{nr} (×10^4 s^{-1})
1	465	631	2.25	0.12	5.4	39.0
2	463	635	2.06	0.14	6.6	41.0
3	461	625	1.67	0.14	7.0	53.0

Cyclic voltammetry was performed in an argon-sparged 0.3 M $LiClO_4/CH_3CN$ solution in a standard three-electrode cell with a platinum disk working electrode. Quasi-reversible waves were found at positive potentials and assigned to the $Ru^{III/II}$ reduction potential (Table 3). Complex **3** was found to have the lowest potential at 1.65 V vs NHE, and **1** had the highest potential at 1.75 V vs NHE. The electrochemistry is termed quasi-reversible because the cathodic and anodic currents were approximately equal while the peak-to-peak separation was

Table 3. Electrochemical Data for 1−3 in a CH_3CN Electrolyte

	$E°$ (V vs NHE)				
complex	ΔG_{ES}	$Ru^{II/+}$	$Ru^{II*/+}$	$Ru^{III/II}$	$Ru^{III/II*}$
1	2.16	−0.68[a]	1.54[b]	1.75	−0.41
2	2.16	−0.69[a]	1.53[b]	1.72	−0.44
3	2.21	−0.71[a]		1.65	−0.56

[a]Irreversible reductions were observed under all conditions investigated; potentials reported are at the peak reductive current. [b]Calculated using the literature value for the first reduction of $[Ru(deeb)_3][PF_6]_2$ dissolved in a CH_3CN electrolyte.[24]

DOI: 10.1021/acs.inorgchem.5b00344
Inorg. Chem. 2015, 54, 4512−4519

greater than 59 mV.[22] Attempts to reduce the complexes resulted in irreversible reduction chemistry at platinum, gold, glassy carbon, or hanging mercury drop working electrodes (Figure S1 in the Supporting Information, SI). A linear region on the high energy edge of the steady-state PL spectra was extrapolated to zero, and the intercept provided the free energy stored in the excited state, ΔG_{ES}.[23] The reducing power of the excited state was calculated as $E°(Ru^{III/II*}) = E°(Ru^{III/II}) - \Delta G_{ES}$. The irreversible nature of the ligand reductions leads to some uncertainty in the oxidizing power of the MLCT excited state. When the literature value for the first reduction of $[Ru(deeb)_3][PF_6]_2$ was used as an approximate value for **1** and **2**, the oxidizing potentials of the excited-state complexes were calculated as $E°(Ru^{II*/+}) = E°(Ru^{II/+}) + \Delta G_{ES}$. The electrochemical data are summarized in Table 3.

Iodide titrations were performed for **1**−**3** in CH_3CN and monitored by UV−vis absorption. Representative data for **1** are given in Figure 3 and those for **2** and **3** in Figure S2 in the SI.

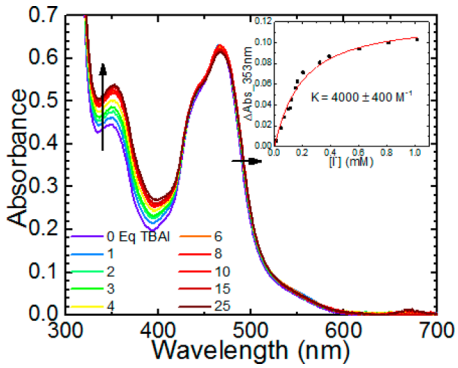

Figure 3. Absorption spectra of **1** with the indicated number of iodide equivalents. The arrows indicate the direction of the absorption change with increasing $[I^-]$. The inset displays the absorption change at 353 nm with an overlaid fit to a nonlinear modified Benesi−Hildebrand model from which an ion pairing equilibrium constant of $K = 4000 \pm 400\ M^{-1}$ was abstracted.

All three complexes displayed a small red shift in the low-energy MLCT absorption upon the addition of iodide. A more significant absorption growth was observed near 360 nm and was analyzed by a nonlinear modified Benesi−Hildebrand equilibrium model, which was previously used to quantify ion pairing equilibrium constants.[25] The abstracted equilibrium constants are reported in Table 4. The concentration of solvated iodide, i.e., "free" or non-ion paired iodide, was determined from the equilibrium constant abstracted from Benesi−Hildebrand analysis.

Iodide was also found to quench the PL intensity and excited-state lifetimes of complexes **1**−**3** in CH_3CN. Representative data are shown for complex **1** in Figure 4. Stern−Volmer plots of the steady-state PL data were nonlinear with upward curvature, behavior that is often observed when both static and dynamic quenching mechanisms are operative. Static quenching was indicated through the decreases in the initial time-resolved PL amplitude (I_0) measured after pulsed-laser excitation. Stern−Volmer analysis of I_0 provided an estimate of the ground-state ion pairing equilibrium constant (K_s) for **1**. This value, $K_S = 14000\ M^{-1}$, was considerably larger than that estimated by the Benesi−Hildebrand-type analysis of the ground-state absorption. A Stern−Volmer plot of the excited-state lifetime for **1** as a function of free iodide was also linear and revealed the dynamic quenching constant K_D (Figure 4). However, the same analysis for **2** and **3** resulted in nonlinear Stern−Volmer plots for both static and dynamic components (Figure S3 in the SI). The reasons for this nonlinearity are uncertain, but it may result from an inability to determine the free iodide concentration with these more highly charged complexes. A bimolecular quenching rate constant (k_q) of $6.27 \times 10^{10}\ M^{-1}\ s^{-1}$ ($k_q = K_D/\tau_0$) was calculated from the dynamic quenching constant measured for **1** and the excited-state lifetime. This value is very close but slightly less than that previously reported for diffusion-limited electron transfer, $k_{diff} = 6.4 \times 10^{10}\ M^{-1}\ s^{-1}$.[24]

Iodide titrations were also monitored by ^1H NMR in CD_3CN. Representative data for **1** are included in Figure S4 in the SI. Large downfield shifts were observed for the H atoms on the tmam ligand after the addition of $^1/_2$ equiv of TBAI to **1**−**3**. The magnitudes of the shifts were dependent on the iodide concentration but saturated after the addition of 10 equiv of iodide. The 3 and 3′ H atoms on the tmam ligands showed the largest shifts (∼1.0 ppm) for all three complexes. Representative data for **1** are given in Figure 5. In neat acetonitrile, the resonances from the H atoms on the methylene C atom that separates the amine from the bipyridine ring were singlets. As iodide was added to the solution, the individual proton resonances appeared, as was indicated by the appearance of two roofed doublets. The coupling constants for each doublet, $J = 14$ Hz, aligned with known methylene proton constants.[26] Relatively large shifts were also seen in the 5, 5′, 6, and 6′ tmam H atoms. In contrast, resonances associated with the deeb ligands in **1** or **2** were essentially independent of the iodide concentration. The magnitudes of the downfield shifts at 6 equiv of I^- for **1** are shown in Figure 6.

Table 4. Equilibrium Constants for Ion Pairing in CH_3CN

complex	UV−vis (K, M^{-1})[a]	PL (K_S, M^{-1})
1	4000	14000
2	4400	*b*
3	7000	*b*

[a]Determined from Benesi−Hildenbrand modeling of the UV−vis absorption changes. [b]Nonlinear Stern−Volmer plots.

DISCUSSION

The synthesis of new highly charged ruthenium complexes based on the tmam ligand was successful. To our knowledge, complex **3** is the most highly charged mononuclear ruthenium(II) complex that has been synthesized, with an overall charge of 8+. Interestingly, the homoleptic **3** maintains a D_3 symmetry over the entire complex including the amines in the solid state. Complexes **1** and **2** have ethyl ester groups that can be hydrolyzed for binding to TiO_2 in future studies. The quaternary amine groups were found to influence the redox and photophysical properties of the complexes as well as the interactions with iodide. This behavior is described below in the context of the relevant literature.

Redox and Photophysical Properties. The redox, structural, and photophysical properties of the newly synthesized and highly charged complexes can largely be understood by consideration of the electronic influence of the substituents in the 4 and 4′ positions of the bipyridine ligands tmam and deeb. The methylene bridge that links the bipyridine to the quaternary N atom in tmam isolates the cationic trimethylamine group from the π system of the bipyridine

DOI: 10.1021/acs.inorgchem.5b00344
Inorg. Chem. 2015, 54, 4512−4519

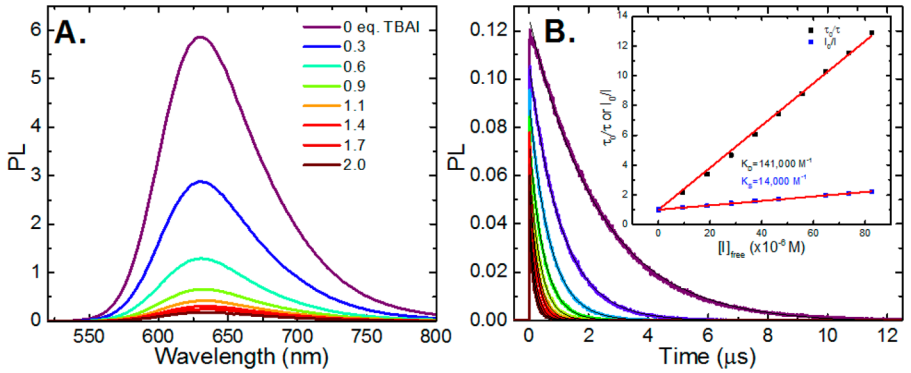

Figure 4. Steady-state (A) and time-resolved (B) PL spectral changes with increasing [I$^-$] for **1**. Inset: Lifetime (black) and intensity (blue) Stern–Volmer plots with overlaid best fits (red lines) for **1**.

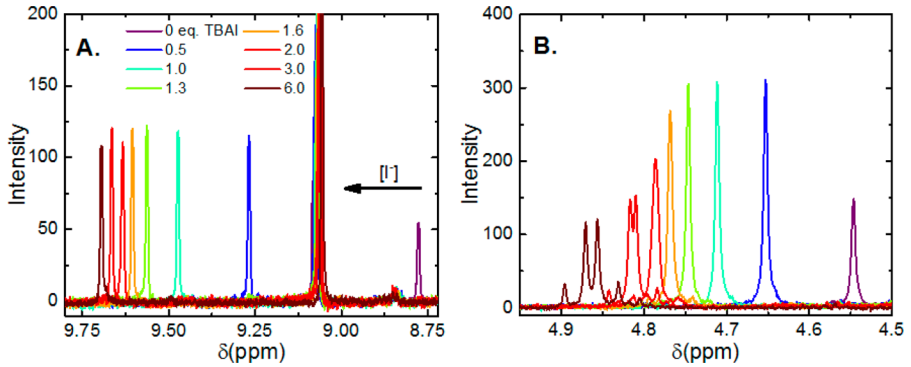

Figure 5. ^{1}H NMR resonances for 3 and 3′ (A) and methylene (B) tmam H atoms of **1** in CD_3CN with the indicated equivalents of iodide.

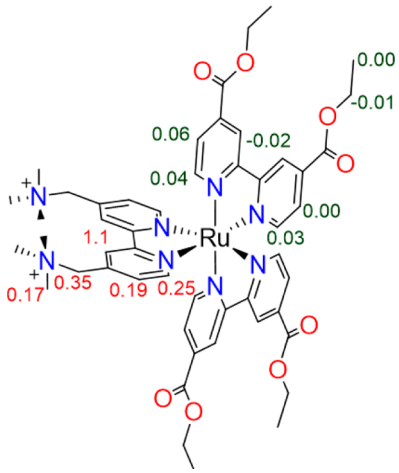

Figure 6. Downfield shifts in ppm for the indicated positions of the H atoms measured at high iodide concentrations, 6 equiv, relative to neat acetonitrile. The deeb ligands were equivalent on the NMR time scale at ambient temperature, and only one is depicted here for clarity.

ligand. The methylene bridge is electron-donating relative to the electron-withdrawing ethyl ester groups of the deeb ligand. These inductive effects were clearly reported by the $E°(Ru^{III/II})$ reduction potentials that shifted 20–70 mV negative when a deeb ligand was replaced with a tmam ligand. Clearly, the tmam ligand provides more electron density to the Ru metal center than does the deeb ligand.

The absorption spectra of the complexes were typical of ruthenium(II) diimine complexes with intense MLCT absorption bands centered in the visible region near 460 nm.[27] The complexes displayed room temperature PL with excited-state lifetimes of a few microseconds. Pioneering resonance Raman studies by Woodruff and co-workers have provided compelling evidence that the excited state of $Ru(bpy)_3^{2+}$ is localized on a single ligand.[28] For heteroleptic ruthenium(II) diimine complexes, Blakley and DeArmond have shown that the excited state localizes upon the ligand that is most easily reduced.[29] The irreversible nature of the ligand reductions for these complexes precluded such a determination. However, solely on the basis of the mesomeric electron-withdrawing effect of the ester group relative to the inductive effect of the tmam ligands, the deeb ligand should be reduced first and therefore be the location for excited-state localization. However, one could envision that Coulombic interaction on the tmam ligand would stabilize the MLCT excited state further by virtue of the cationic charge present. Hence, there was some concern that complexes **1** and **2** could be an exception to DeArmond's rule. While the data do not provide definitive proof of where the excited state is localized, there is strong evidence that it is localized on a deeb ligand in the heterolpetic ruthenium(II) complexes **1** and **2**.

The free energy stored in the MLCT excited state is proportional to the energy separation between the metal-based $E°(Ru^{III/II})$ and the first ligand reduction $E°(Ru^{II/+})$. To a very good approximation, the first ligand reduction potentials are insensitive to the identity of the other diimine ligands or even the metal ion that it is coordinated to.[27] With this in mind, consider complex **3**, whose excited state is well formulated as $[Ru^{III}(tmam^-)(tmam)_2]^{8+*}$ and stores about 2.21 eV of free energy in the excited state with $E°(Ru^{III/II})$ = 1.65 V vs NHE. As mentioned above, the $E°(Ru^{III/II})$ potentials shift positively when a tmam ligand is replaced by deeb. Therefore, if the

DOI: 10.1021/acs.inorgchem.5b00344
Inorg. Chem. 2015, 54, 4512–4519

Scheme 3. Proposed Mechanism for Iodide Photooxidation by 1, Where N−N = deeb

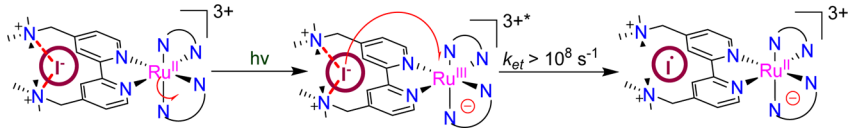

excited state were localized on the tmam ligand in **1** or **2**, the corresponding PL spectra would be shifted to higher energy, contrary to the experimental data. The lower-energy PL from **1** and **2** is, hence, most consistent with radiative relaxation from an excited state localized on the deeb ligand. Additional, albeit indirect, evidence for a deeb-localized excited state comes from the significantly longer lifetimes of **1** and **2** (2.25 and 2.06 μs, respectively) relative to **3** (1.67 μs). It has previously been noted that $[Ru^{III}(deeb^{-})(LL)_2]^{2+*}$ complexes possess longer-lived excited states than related complexes with similar energy gaps, a behavior that has been attributed to delocalization over the ethyl ester group in the MLCT excited state.[30]

Therefore, the thermally equilibrated excited states of complexes **1** and **2** are well formulated as an oxidized Ru center and a reduced deeb ligand. This is shown for complex **1** in eq 1.

$$Ru^{II}(deeb)_2(tmam)^{4+} + h\nu \rightarrow [Ru^{III}(deeb^{-})(deeb)(tmam)]^{4+*} \quad (1)$$

Localization of the excited state on the ligand that interacts with the TiO_2 surface is likely important for future studies in dye-sensitized solar cells. It also has significance for iodide photooxidation because the excited state is localized away from the quaternary amines that interact with iodide, as is discussed below.

Iodide Interactions. Taken together, the results of NMR, PL, and UV−vis absorption spectroscopy provide compelling evidence that iodide forms ion pairs with these cationic complexes in acetonitrile. Under the same conditions, there was no evidence for ion pairing of $Ru^{II}(deeb)(bpy)_2^{2+}$ with iodide.[31] This suggests that the increased cationic charge of the tmam-containing complexes was responsible for ion pairing. Indeed, the tmam ligand was designed to facilitate ion pairing through iodide's interactions with the cationic charges of the quaternary amine.

To investigate the details of iodide interactions with these complexes, ^{1}H NMR was utilized. The furthest downfield resonances of the tmam ligand in all of the complexes corresponded to the 3 and 3′ H atoms on the bipyridine ring. These 3 and 3′ resonances shifted further downfield, by more than 1 ppm, as iodide was titrated into the solution. This downfield shift was previously reported for halide ion pairing in related dicationic ruthenium(II) heteroleptic complexes in DCM solutions.[25,32] The electronegative iodide interacts with the most acidic electropositive H atom, drawing it away from the bipyridyl C atom and effectively deshielding it. This effect was also "felt" by the other protons on the bipyridine rings of tmam, which show significant yet smaller downfield shifts (~0.3−0.4 ppm). In contrast, the resonances associated with the deeb ligand were largely insensitive to the addition of iodide.

A key insight into the interactions of iodide resulted from analysis of the methylene C protons that link trimethylamine to the bipyridine ring. Because the ruthenium complexes are chiral, these methylene protons are diastereotopic, and doublets are expected. However, in neat acetonitrile, they appeared as a singlet, presumably because the average magnetic environment for each H atom (on the same C) was equivalent. As iodide was titrated into the solution, these singlets split into two roofed doublets as the diastereotopic coupling emerged, indicating that the magnetic environments were no longer equivalent. The downfield shifts of the methyl (~0.2 ppm) and methylene (~0.4 ppm) protons on the tmam ligand were significant and provide clear evidence that iodide was indeed interacting with the quaternary amine.

The results of the ^{1}H NMR titrations indicated that iodide was stabilized by the 3 and 3′ H atoms of the bipyridine ring and the methylene and methyl groups of the tmam ligand. An iodide "binding pocket" can be envisioned where iodide forms an adduct by interacting with the acidic 3 and 3′ H atoms of the tmam ligand and is further stabilized by the trimethylamine groups, which can wrap around the iodide. An example of this is shown in Scheme 3. This adduct gives rise to a nonemissive excited state that appears as a static component in the excited-state relaxation, consistent with rapid electron transfer from iodide to the metal center, $k_{et} > 10^8$ s^{-1}. Given the accepted $E°(I^{0/-}) = 1.23$ V vs NHE reduction potential in CH_3CN, the reaction is endergonic by 0.31 eV.[33] At low iodide concentrations, a dynamic process was also observed for **1**, consistent with a second-order rate constant of 6.3×10^9 M^{-1} s^{-1} that is about an order of magnitude smaller than that calculated for the diffusion limit, yet consistent with the known rapid redox reactivity of iodide.[33] The rapid static electron transfer and identification of a iodide "binding pocket" on the tmam ligand suggests that these complexes will be of use for application in dye-sensitized solar cells and may indeed enhance regeneration at the power point, where the electric field is strong and regeneration by iodide is inhibited.[34,35]

CONCLUSION

Three new highly charged cationic ruthenium(II) complexes were successfully prepared and characterized based on the tmam ligand. Two of these complexes had ester functional groups that can be hydrolyzed for sensitization of metal oxide electrodes. The third complex was ligated to three tmam ligands with high symmetry in the solid state and an overall 8+ charge, making it the most highly charged mononuclear ruthenium(II) complex ever prepared. The high cationic charge resulted in significant ion pairing with low concentrations of iodide in polar CH_3CN solutions, a behavior that was absent for related ruthenium(II) bipyridyl complexes with a 2+ charge. NMR studies revealed that, by virtue of a unique "binding pocket", iodide preferentially interacts with the tmam ligand over diethyl ester bipyridine ligands. Iodide photooxidation occurred rapidly, $k > 10^8$ s^{-1}, as was inferred by a static component in excited-state quenching measurements. The data demonstrate that electrostatics and acid−base chemistry can be used to assemble well-characterized adducts of iodide and transition-metal complexes in polar solvents. Such behavior is important for optimizing the rates of photoinduced electron transfer relative to excited-state relaxation and may help

DOI: 10.1021/acs.inorgchem.5b00344
Inorg. Chem. 2015, 54, 4512−4519

overcome the mass-transport limitations that occur in dye-sensitized solar cells when high solar fluxes are employed.

■ ASSOCIATED CONTENT

Supporting Information

CIF file for **3**, cyclic voltammograms for **1**−**3**, absorption spectra and nonlinear Stern−Volmer analysis for **2** and **3**, and full NMR titrations for **1**. This material is available free of charge via the Internet at http://pubs.acs.org.

■ AUTHOR INFORMATION

Corresponding Author

*E-mail: gjmeyer@email.unc.edu.

Notes

The authors declare no competing financial interest.

■ ACKNOWLEDGMENTS

The Division of Chemical Sciences, Geosciences, and Biosciences, Office of Basic Energy Sciences of the U.S. Department of Energy, through Grant DE-FG02-96ER14662 is gratefully acknowledged for support. Peter White assisted with X-ray crystallography, and Marc ter Horst assisted with NMR spectroscopy. Javier Grajeda and the laboratory of Prof. A. J. M. Miller assisted with ESI-MS and synthetic discussion.

■ REFERENCES

(1) Sutin, N. *Acc. Chem. Res.* **1982**, *15*, 275.
(2) Ardo, S.; Meyer, G. J. *Chem. Soc. Rev.* **2009**, *38*, 115.
(3) Pelet, S.; Moser, J.-E.; Grätzel, M. *J. Phys. Chem. B* **2000**, *104*, 1791.
(4) Redmond, G.; Fitzmaurice, D. *J. Phys. Chem.* **1993**, *97*, 1426.
(5) Kelly, C. A.; Farzad, F.; Thompson, D. W.; Stipkala, J. M.; Meyer, G. J. *Langmuir* **1999**, *15*, 7047.
(6) O'Donnell, R. M.; Ardo, S.; Meyer, G. J. *J. Phys. Chem. Lett.* **2013**, *4*, 2817.
(7) Boschloo, G.; Hagfeldt, A. *Acc. Chem. Res.* **2009**, *42*, 1819.
(8) Nazeeruddin, M. K.; Zakeeruddin, S. M.; Humphry-Baker, R.; Jirousek, M.; Liska, P.; Vlachopoulos, N.; Shklover, V.; Fischer, C.; Grätzel, M. *Inorg. Chem.* **1999**, *38*, 6298.
(9) Qu, P.; Meyer, G. J. *Langmuir* **2001**, *17*, 6720.
(10) Finnie, K.; Bartlett, J.; Woolfrey, J. *Langmuir* **1998**, *7463*, 2744.
(11) Umapathy, S.; Cartner, A. M.; Parker, A. W.; Hester, R. E. *J. Phys. Chem.* **1990**, *94*, 8880.
(12) Němec, H.; Rochford, J.; Taratula, O.; Galoppini, E.; Kužel, P.; Polívka, T.; Yartsev, A.; Sundström, V. *Phys. Rev. Lett.* **2010**, *104*, 197401.
(13) Clifford, J. N.; Palomares, E.; Nazeeruddin, M. K.; Gratzel, M.; Durrant, J. R. *J. Phys. Chem. C* **2007**, *111*, 6561.
(14) Gillaizeau-Gauthier, I.; Odobel, F.; Alebbi, M.; Argazzi, R.; Costa, E.; Bignozzi, C. A.; Qu, P.; Meyer, G. J. *Inorg. Chem.* **2001**, *40*, 6073.
(15) Dolomanov, O.; Bourhis, L. J.; Gildea, R.; Howard, J. A. K.; Puschmann, H. *J. Appl. Crystallogr.* **2009**, 339.
(16) Bourhis, L. J.; Dolomanov, O. V.; Gildea, R. J.; Howard, J. A. K.; Puschmann, H. *Acta Crystallogr., Sect. A* **2015**, 59.
(17) Sheldrick, G. M. *Acta Crystallogr., Sect. A* **2008**, 112.
(18) Crosby, G. A.; Demas, J. N. *J. Phys. Chem.* **1971**, *75*, 991.
(19) Pavlishchuk, V. V.; Addison, A. W. *Inorg. Chim. Acta* **2000**, *298*, 97.
(20) Li, J.-H.; Wang, J.-T.; Hu, P.; Zhang, L.-Y.; Chen, Z.-N.; Mao, Z.-W.; Ji, L.-N. *Polyhedron* **2008**, *27*, 1898.
(21) Yu, Z.; Najafabadi, H. M.; Xu, Y.; Nonomura, K.; Sun, L.; Kloo, L. *Dalton Trans.* **2011**, *40*, 8361.
(22) Bard, A.; Faulkner, L. *Electrochemical Methods Fundamentals and Applications*; John Wiley & Sons, Inc.: Hoboken, NJ, 2001.
(23) Adamson, A. W.; Namnath, J.; Shastry, V. J.; Slawson, V. *J. Chem. Educ.* **1984**, *61*, 221.
(24) Farnum, B. H.; Jou, J. J.; Meyer, G. J. *Proc. Natl. Acad. Sci. U. S. A.* **2012**, *109*, 15628.
(25) Ward, W. M.; Farnum, B. H.; Siegler, M.; Meyer, G. J. *J. Phys. Chem. A* **2013**, *117*, 8883.
(26) Friebolin, H. *Basic One- and Two-Dimensional NMR Spectroscopy*; Wiley-VCH: Hiedelberg, Germany, 2011.
(27) Kalyanasundaram, K. *Photochemistry of polypyridine and porphyrin complexes*; Academic Press: San Diego, CA, 1992.
(28) Bradley, P.; Kress, N. *J. Am. Chem. Soc.* **1981**, 1441.
(29) Blakley, R.; DeArmond, M. *J. Am. Chem. Soc.* **1987**, 4895.
(30) Taheri, A.; Meyer, G. J. *Dalton Trans.* **2014**, *43*, 17856.
(31) Marton, A.; Clark, C. C.; Srinivasan, R.; Freundlich, R. E.; Narducci Sarjeant, A. a.; Meyer, G. J. *Inorg. Chem.* **2006**, *45*, 362.
(32) Beer, P.; Dent, S.; Wear, T. *J. Chem. Soc., Dalton Trans.* **1996**, *1*, 2341.
(33) Rowley, J. G.; Farnum, B. H.; Ardo, S.; Meyer, G. J. *J. Phys. Chem. Lett.* **2010**, *1*, 3132.
(34) Robson, K. C. D.; Hu, K.; Meyer, G. J.; Berlinguette, C. P. *J. Am. Chem. Soc.* **2013**, *135*, 1961.
(35) Li, F.; Jennings, J. R.; Wang, Q. *ACS Nano* **2013**, *7*, 8233.

DOI: 10.1021/acs.inorgchem.5b00344
Inorg. Chem. 2015, 54, 4512−4519